Construction and Testing of an Atmospheric-Pressure Transmission-Mode Matrix Assisted Laser Desorption Ionisation Mass Spectrometry Imaging Ion Source with Plasma Ionisation Enhancement

Rory T. Steven[†,*], Michael Shaw[¥,τ], Alex Dexter[†], Teresa Murta[†], Felicia M. Green[†], Kenneth N. Robinson[†], Ian S. Gilmore[†], Zoltan Takats[Ω], and Josephine Bunch[†, Ω, *]

[†]: National Centre of Excellence in Mass Spectrometry Imaging (NiCE-MSI), Analytical Science Division, National Physical Laboratory (NPL), Teddington, UK, TW11 0LW, UK

[¥:] Biotechnology Group, Analytical Science Division, National Physical Laboratory, Teddington, TW11 0LW, UK

[τ]: UCL Touch lab, Department of Computer Science, University College London, Gower Street, London, WC1 6BT, UK

[Ω]: Imperial Collage London, Faculty of Medicine, Department of Surgery & Cancer, London, SW7 2AZ, UK

*: Corresponding authors: Rory Steven, email: rory.steven@npl.co.uk, telephone: +44 (0)2089 436 420; Josephine Bunch: email: josephine.bunch@npl.co.uk, telephone: +44 (0)2089 436 509

Abstract

Matrix assisted laser desorption ionisation mass spectrometry (MALDI-MS) at atmospheric pressure (AP) is, with a few notable exceptions, overshadowed by its vacuum based forms and AP transmission mode (TM) MALDI-MS lacks the up-take its potential benefits might suggest. The reasons for this are not fully understood and it is clear further development is required to realise the flexibility and power of this ionisation method and geometry. Here we report the build of a new AP-TM-MALDI-MSI ion source with plasma ionisation enhancement. This novel ion source is used to analyse a selection of increasingly complex systems from molecular standards to murine brain tissue sections. Significant enhancement of detected ion intensity is observed in both positive and negative ion mode in all systems, with up to 2000 fold increases observed for a range of tissue endogenous species. The substantial improvements conferred by the plasma enhancement are then employed to demonstrate the acquisition of proof of concept tissue images, with high quality spectra obtained down to 10 × 10 µm pixel size.

1. Introduction

MALDI-MS is used to analyse a large range of molecular classes in a wide variety of sample types and applications. Despite this, great effort is still being made to expand the utility and efficacy of MALDI-MS and MSI to enable improved limits-of-detection, variety of sample types and extend its flexibility of application. MALDI-MS is typically carried out under vacuum conditions with front-side (reflection-geometry) laser irradiation. Whilst providing benefits this arrangement also restricts the practitioner in what can be achieved or implemented. For example, a number of recently published post-ionisation methods such as plasma [1] or electrospray [2] cannot typically operate under vacuum conditions and the form and location of the laser focussing lens is restricted by the MALDI plume ejection from the sample surface.

Laser desorption MS and MALDI-MS ion sources operated under vacuum conditions until around 2000 when Laiko *et al.* demonstrated the first AP-MALDI-MS ion source, coupled to an orthogonal time-of-flight (ToF) instrument [3]. Recently, exciting data showing generation of multiply charged species has been demonstrated in ion sources of this form [4, 5]. The current state of the art with regards to AP-MALDI-MSI is the high resolution ion source developed by the Spengler group [6-8]. This source is coupled to Orbitrap type instruments and is able to collect high quality imaging data with pixel sizes below 10 µm. Significantly, intermediate pressure ion sources are gaining renewed interest in recent years , perhaps pointing to increased utility of higher pressure ion source operation than was previously assumed.

AP or ambient ionisation can provide flexibility for the incorporation of additional functionality. One potentially significant advantage of AP sources is their ease of coupling with additional ionisation methods. Numerous plasma devices have been proposed and evidenced as useful for ionisation in mass spectrometry including: corona discharge (DART, ASAP), glow discharge (PADI, MHCD) and dielectric barrier discharge (DBDI, LTP)[9]. These various plasma forms and methods of production give rise to differing plasma properties including temperature and nature of electrical properties exhibited. Plasma assisted desorption ionisation (PADI) is a low temperature (largely non-thermal) form which has now been studied by a number of groups [1, 10-12]. Despite possible limitations

regarding desorption from surfaces, plasma ionisation shows promise as an ionisation tool for molecules in the gas phase or which desorb easily due to, for example, a low vapour pressure [13, 14]. The Zenobi group has also demonstrated an elegant solution to the introduction of a plasma source into an AP-LDI / MALDI setup by building it into the ion transfer capillary [1].

TM-MALDI-MS under vacuum has been successfully revisited recently for imaging applications by the Caprioli group [15, 16], where peptide and lipid mass spectral data have been acquired with 1 µm pixel sizes. The benefit of the TM geometry in this context is to enable a high numerical aperture (NA) lens, with a correspondingly short working distance, to be mounted sufficiently close to the sample without blocking the path of the MALDI-MS ablation plume, allowing the potential for smaller irradiated regions.

The Trimpin group reported AP-TM-MALDI-MS profiling of murine brain tissue sections with the use of CHCA and 2,5-DHB [17]. The first example of AP-TM-MALDI-MS imaging was subsequently published by the Trimpin group in 2011 [18]. More recently an unusual combination of femtosecond, near-infrared, 75 MHz repetition rate laser with a gold nanoparticle matrix and plasma post-ionisation was used for tissue imaging; showing potentially powerful results in the context of native tissue analysis [19]. Despite this and despite the fact that AP-TM-MALDI-MS was first carried out ~15 years ago [20], there has been no wide-scale take-up of this instrumental setup and there are no commercially available ion sources operate in this manner. This is despite a number of potential benefits including: ease and flexibility of coupling to existing instruments; the ability to readily alter laser focussing and monitor energy; relative simplicity of introducing post ionisation strategies and the possibility for analysis of samples in their native state.

Previously published work incorporating AP-TM-MALDI-MS suggests possible issues with: limit-of-detection (LoD); ion transmission from atmosphere to vacuum; differences in ionisation mechanisms and greater variance within the acquired data. These may all be contributing phenomena with regards to the lack of utility and take-up of AP-TM-MALDI-MS [3, 20, 21].

Within this study a 3-axis sample translation stage is modified to enable atmospheric pressure transmission mode laser irradiation of samples and is coupled to an Orbitrap MS instrument, creating an AP-TM-MALDI-MS imaging ion source. Additionally, a previously developed plasma device [14] is incorporated into the ion source to provide post ionization signal enhancement. A selection of molecular standards and murine tissue are analysed in both positive and negative ion mode to establish the utility of this source and the efficacy of plasma enhancement therein. The ion source is then used to acquire proof of concept plasma enhanced AP-TM-MALDI-MS images from murine brain at 50 × 50 µm and 10 × 10 µm pixel size.

2. Methods

2.1. Materials

Methanol (LC-MS grade), Fisher Scientific (Leicestershire, UK); purified water, ELGA Purelab Option (Marlow, UK); Lipid standard phosphatidylcholine (PC) 16:0/18:1, Avanti Polar Lipids (Delfzyl, The Netherlands); Trifluoroacetic acid (TFA), Acros Organics (Loughborough, UK); MALDI matrices and analytes 2,6-dihydroxyactophenone (2,6-DHAP), histidine, glutamic acid, amiodarone, insulin,

probucol, choline chloride, fumaric acid, cysteine, ketoglutaric acid, glutamic acid, dopamine hydrochloride, l-histidine, tryptophan, ibuprofen, palmitic acid, glucose 6 phosphate, glutathione, clozapine, glycochenodeoxycholate, raffinose, probucol, amiodarone, co-enzyme Q10, ubiquitin (from bovine erythrocytes) were purchased from Sigma Aldrich (Dorset, UK) at 98% purity or above. Paclitaxel and rapamycin from Alfa Aesar (Lancashire, UK). Superfrost Plus (Thermo Scientific, Waltham, MA, USA) glass slides were used for all experiments.

2.2. Sample Preparation

Drug standards and DHAP for experiments shown in Section 3.2 were all prepared at 1 and 10 mg mL^{-1} respectively, in 80 % methanol 20% water and then mixed 1:1 (*v:v*) prior to pipetting. In the case of the dried droplet experiments 0.2 µL was pipetted. The 19 standard solution described in Section 3.3 was prepared at concentrations shown in SI Table 1 and mixed 1:2 with DHAP prior to deposition by TM Sprayer (HTX Technologies, North Carolina (NC), USA). The settings used were: 13 passes, 0.07 mL $minute^{-1}$ flow rate, 3 mm track spacing, 65 ° C, 15 psi nitrogen pressure, 1.5 mm offset and rotation applied alternately.

2.3. Optics Setup and Laser Energy Monitoring

An Nd:YAG laser (355nm output wavelength, FQS series, Elforlight Ltd. Daventry, UK) coupled into a 100 µm core diameter fibre (Fiberguide Industries, NJ, USA) as previously described [22, 23] within section 3.2 and as a free space beam in subsequent sections. A laser energy of approximately 12 µJ laser energy per pulse at the sample slide surface at 1000 Hz was used for tissue imaging experiments. This energy was determined by placing a blank slide into the sample position and irradiating it as during data acquisition, a laser energy meter is then introduced to the ions source between this sample slide and the inlet capillary (having moved the stage back to accommodate it). Thus a true 'on sample' energy measure is made. A x0.5 image of the fibre end face was projected through the sample slide onto the front face using a pair of UV fused silica plano-convex lenses mounted in a 4f relay configuration (focal lengths 50 mm and 100 mm, Thorlabs, Ely, UK). To minimise reflection losses both lenses were coated with a UV antireflection coating. A beamsplitter (BSF10-C, Thorlabs, Ely, UK) mounted before the first relay lens deflected 1% of the light to a PD10-C energy sensor (Ophir Photonics, Darmstadt , Germany) for online laser energy monitoring.

2.4. Transmission Mode Ion Source Stage

A developmental desorption electrospray ionisation (DESI) ion source ("3D stage", Prosolia Inc, Indianapolis, IN, USA) designed to couple to Thermo Orbitrap type mass spectrometers was modified to enable the attachment of optical components. Firstly, the motorized x, y, z stage was shifted laterally on its base plate to create an obstructed path and allow axial of alignment of the laser and inlet capillary of the mass spectrometer. A microscope slide holder (MAX3SLH, Thorlabs, Ely, UK) was then attached to the side of the stage, to allow positioning of the sample perpendicular to the inlet capillary and laser illumination. A CCD camera (DCU223M, Thorlabs, Ely, UK) was mounted coaxially to the laser optics to provide an image of the sample surface. The stage was controlled through the supplied Prosolia software (Omnispray). To trigger the laser appropriately for automated analysis the existing peripheral control electronics of the Orbitrap were used. The 'Start In' and 'Ready Out' connections which provide TTL triggering voltages for the stage movement were utilised to additionally provide the laser trigger signal.

2.5. Plasma Source

The plasma source used here was as previously described [14]. Briefly, the plasma device was constructed from an outer glass capillary containing a ceramic tube insulating a tungsten wire with sharpened tip. A grounded copper electrode encircles the outer glass capillary approximately 4 mm from the plasma generating end of the device. A RFG050 radio frequency generator, operating at 13.56 MHz, was used in conjunction with an AMN150R automatic matching network (Coaxial Power Systems, UK) to drive the plasma device. The power was set to 13W for all experiments. Helium (99.996%, BOC, UK) was used as the discharge gas at a flow rate of approximately 820 mL min^{-1}.

2.6. Mass Spectrometry

An LTQ Orbitrap Elite converted from Velos (Thermo Scientific, Waltham, MA, USA) mass spectrometer was used and operated in positive ion mode at the manufacturer's 120,000 mass resolving power setting with the automatic gain control (AGC) turned off. A stainless steel inlet capillary of ~ 14 cm total length and ~ 8 cm from instrument inlet, supplied by Prosolia, was used. The inlet temperature was set to 300 degrees centigrade and the capillary heating to 350 degrees centigrade. Analysis of the 19 compound mixture: 0.05 mm s^{-1} stage speed, 120,000 mass resolving power setting, 500 ms injection time setting, analysis for 1mm raster giving 47 pixels per data set which equates to effective pixel size of approximately 22 µm wide pixel with 50 µm high ablated region giving pixel area of $1.1x10^{-9}$ m^2. Analysis of tissue was carried out with the following settings: single tissue raster line sampling and 50 µm or 10 µm pixel size images: resolution 120,000, injection time 100ms, stage speed 100 µm s^{-1} or 20 µm s^{-1} with y-axis step size of 50 µm or 10 µm, aiming to provide images with pixel size of either 50 µm or 10 µm in the x-axis. Stage stepping was set to provide the y-axis pixel dimension. The injection time here resulted in approximately 130 scans per minute (0.46 per second) as shown in the total ion chromatograms in Thermo Excalibur software. This gives rise to effective pixel sizes of approximately 44 µm x 50 µm and 9 µm x 10 µm in the presented images. During these analyses it was evident that setting the mass spectrometer to record from a broad *m/z* range significantly compromised the LODs at the higher end of the mass range, likely due to space charging and dynamic range effects within the iontrap and orbitrap regions of the mass spectrometer due to the large number of plasma ion in the low *m/z* range (SI Figure S1). Therefore, these and subsequent analyses were split up into the smaller *m/z* ranges shown. MS/MS data was collected with a 1 Da window and the collision energy was optimised whilst data was collected with continuous raster sampling of the tissue with the plasma enhancement turned on to ensure sufficient parent ion signal.

2.7. Data Processing

The proprietary .raw data files were converted to mzML using msconvert from ProteoWizard [24]. These mzML files were then converted to imzML using imzMLConverter [17] and processed by SpectralAnalysis [25] within MATLAB (ver. R2017a, MathWorks Inc., MA, USA). Assignment to the human metabolome database (HMDB) [26] was carried out from peak picked data (gradient descent method) compared against a variety of possible adduct forms from the isotopic masses within HMDB within ± 2ppm above a defined noise threshold.

3. Results and Discussion

3.1. Ion source design, construction and initial testing

An existing developmental DESI stage was modified to incorporate transmission geometry illumination to carry out AP-TM-MALDI-MS. A schematic and photographs of the optics and source setup developed within this study is shown in Figure 1.

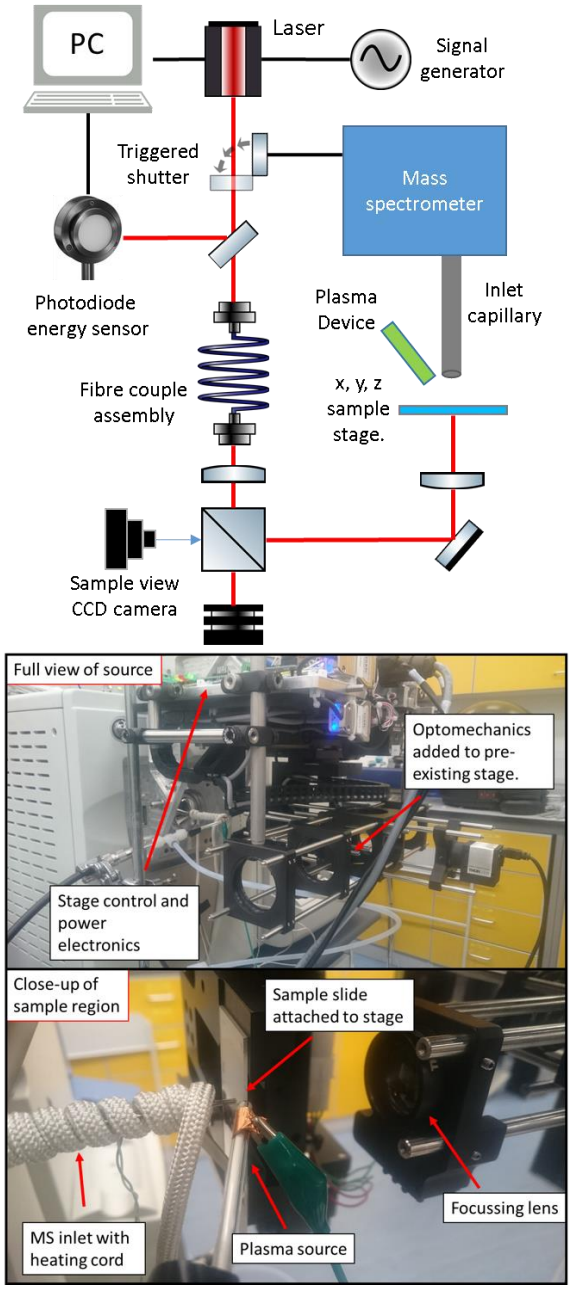

Figure 1. Schematic of AP-TM-MALDI ion source setup used within this study with labelled photographs below.

The motorized x, y, z stage operates with the x-y plane parallel to the ion inlet block of the mass spectrometer with the z axis of the stage coaxial to the inlet capillary of the mass spectrometer. This setup is therefore amenable to transmission mode sample illumination with modest alteration of the stage design and the addition of necessary optomechanics. The primary considerations for the modified system are: positioning the illumination optics in relation to the sample substrate and mass spectrometer inlet capillary orifice; positioning the existing stage so as to best accommodate a variety of lenses and optomechanics; allowing for the incorporation of additional post ionisation technology; alignment, measurement and modification of laser beam characteristics. Underlying these considerations is an additional requirement to allow for future alteration and upgrades to this setup. Sharing a similar laser triggering setup to that used previously by our group [22, 23, 27], the laser is continuously triggered from a pulse generator at selected repetition rate and a shutter is used to control sample illumination using a TTL voltage trigger signal from the mass spectrometer, which is also used to synchronising instrument spectral acquisition and sample stage movement in Prosolia DESI ion sources, for example. This triggering method can result in improved laser energy stability as the laser is continuously triggered by the signal generator ensuring an approximately steady state thermal control of the laser components [27].

The laser energy incident on the sample is monitored on-line using a 1% beamsplitter in the laser beam path. Energy losses due to refletion and absorption by the down beam optics and the sample substrate were measured off-line to calibrate the reading on the energy meter to the energy incident on the sample itself. Losses through standard microscope glass slide were not found to be significant enough to necessitate the increased cost of quartz substrate. The use of an optical fibre in this was a compromise to enable the safe, convenient delivery of the laser from the nearby optical table bench to the instrument itself. The down sides of fibre use include the relative ease with which they can be damaged, due to suboptimal laser coupling, during an experiment, potentially invalidating any results and necessitating replacement. More fundamentally, the spatially extended, inhomogeneous beam profile at the output of a multimode fibre places a lower limit on the size of the irradiated region. Latterly (sections 3.3 onward) the system was also operated using a fibre free irradiation from laser to ion source optics. The collimating and focussing lens setup can be aligned, altered and changed with relative ease. Additional capillary heating was added in the form of an electrically insulated heating wire wrapped around the inlet capillary enabling heating of the whole inlet capillary rather than only at the ion block itself. Lastly, the open construction around the sample also allows a plasma device to be incorporated into the setup for use as a post-ionisation source.

Preliminary studies with this AP-TM-MALDI ion source were carried out with a view to modifying laser focussing, providing benchmark data for a range of analytes as well as evaluating inlet heating, temperature variation and sample to inlet distance (**Error! Reference source not found.**SI Figures S2 to S4).

The flexibility inherent in this setup allow for features, such as customisable laser optics, not typically found in commercial instruments. Interchanging lenses and using different launch fibres provides a route to adjust the irradiance distribution. The beam diameter employed within these early studies exhibits a D86 (also know as $1/e^2$) diameter of approximately 50 μm (SI Figure S2 and S3). The inlet temperature was investigated and found to be optimum for detection of the lipid PC

34:1 at 300 – 350 °C (Figure S4). Additionally, the inlet to sample distance was optimum at ~ 0.5 mm (Figure S5).

3.2. Analysis of individual compounds

Drug molecules are of particular interest as their detection in biological samples during, for example, mass spectrometry imaging studies, is of critical importance to pharmacokinetic and toxicity assessment of those compounds [28]. Within this study a plasma device previously developed within this group [14, 29] was incorporated into the AP-TM-MALDI-MS ion source whereby the plasma region coincides with the laser sampling region and plume path into the inlet capillary (Figure 1). Spotted samples of amiodarone, paclitaxel, probucol and rapamycin, with DHAP matrix, were analysed with the laser only, with plasma only and with both laser and plasma turned on. A summary of this data is shown in Figure 2 and SI Figure 6**Error! Reference source not found.**.

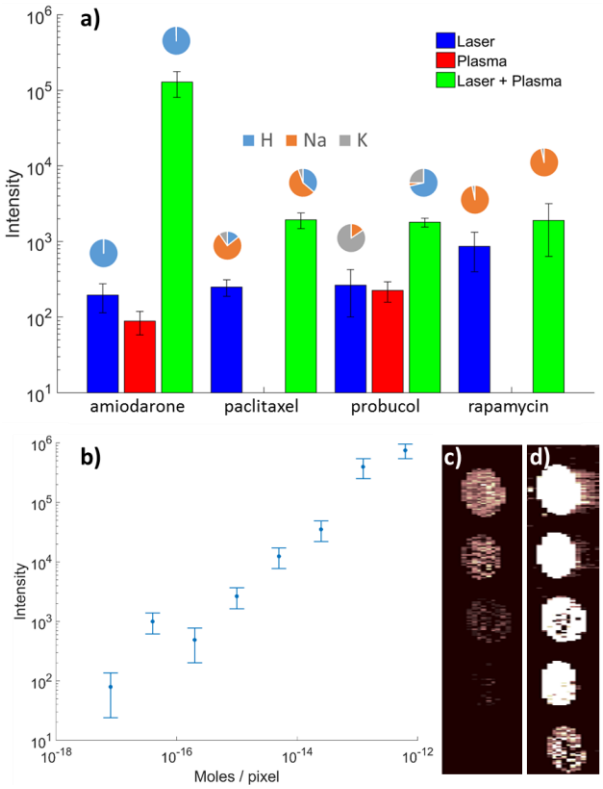

Figure 2. AP-TM-MALDI-MSI with plasma enhancement from drug compounds. **a)** all adduct summed signal from amiodarone, paclitaxel, probucol and rapamycin with and without laser and plasma. The proportion of signal derived from each ion adduct form are shown in pie charts above each corresponding column. **b)** mean ion intensity from serial dilution of amiodarone collected with plasma enhancement. **c)** image of pipetted spots acquired from 5 highest concentration solutions shown in b), **d)** as c) but with intensity scale saturated so low intensity signal is visible.

All of the tested compounds showed an increased mean molecular ion intensity where plasma was used in addition to the laser irradiation (Figure 2 a)Error! Reference source not found.. Amiodarone, paclitaxel and probucol showed significant increase with amiodarone showing the largest increase at approximately 1000-fold. Plasma devices, such as the one used here, have previously been shown to be poor at initiating desorption of lower vapour pressure substances meaning significant detection from typical MALDI-MS matrix compounds is therefore likely to be minimal [13]. Therefore, the use of the MALDI matrix may well help prevent more volatile species leaving the sample surface under action from the plasma, helping retain the spatially defined laser sampling of this technique where the additional plasma is used. Pie charts showing the proportion of each detected compound seen as each charge adduct ($[M+H]^+$, $[M+Na]^+$ or $[M+ K]^+$) are also shown in Error! Reference source not found.above the corresponding data set. In the case of amiodarone, paclitaxel and probucol the $[M+H]^+$ adduct is enhanced to the greatest degree. Error! Reference source not found.As a proof of concept for imaging by AP-TM-MALDI-MS with the addition of plasma enhancement on this system, a serial dilution of amiodarone mixed with DHAP was analysed resulting in moles per pixel within the range 10^{-18} to 10^{-12} (Figure 2 b). These data may be viewed positively as they span a concentration range of five orders of magnitude; a non-trivial range for mass spectrometric data acquisition. The limit-of-detection (LoD) for amiodarone, detected by any laser based mass spectrometry, has not previously been reported but the value of < 100 attomoles per pixel detection shown here is encouraging. The image data shown in Figure 2 c) and d) was also acquired as proof of concept in continuous raster scanning mode. The higher concentration samples possibly show carry-over of amiodarone in adjacent pixels at the highest concentration (Figure 6 c) but reassuringly this is not present in the lower concentrations which would likely be the more relevant for tissue imaging and drug distribution studies.

3.3. Analysis of standards mixture

To further examine the effect of plasma enhancement on this device a mixture of 19 standards was prepared to the concentrations shown in SI Table 1. Single line raster samples were acquired in each polarity across different mass ranges with and without plasma enhancement. Taking into account the effective area of the pixels in these data this resulted in the number of molecules per pixel, also shown in SI Table 1, ranging from 10^{-13} to 10^{-15}. Example mean spectra from these data are shown in Figure 3.

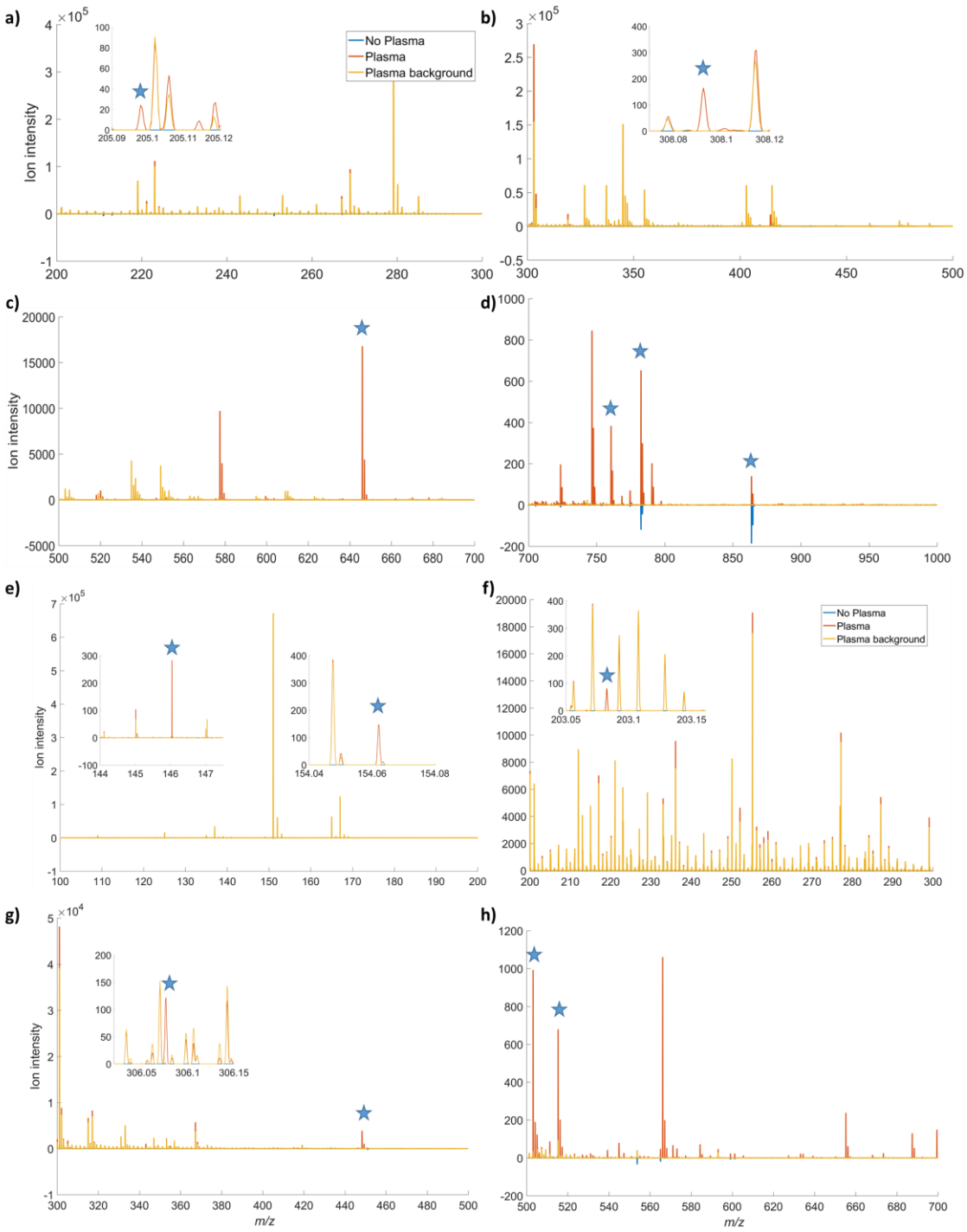

Figure 3. Example spectra from positive (a – d) and negative (e – h) ion mode analyses of standards mixture both with and without plasma enhancement. Colour key: blue – without plasma; red – with plasma; yellow – plasma background. Data without plasma multiplied by -1 to aid visualisation. Starred ions indicate detected standards, in ascending charge and *m/z* order as follows: **a)** tryptophan $[M+H]^+$; **b)** glutathione $[M+H]^+$, **c)** amiodarone $[M+H]^+$, **d)** PC 34:1 $[M+H]^+$, $[M+Na]^+$, co-enzymen Q10 $[M+H]^+$; **e)** ketoglutaric acid $[M+H]^+$, histidine $[M+H]^+$; **f)** tryptophan $[M+H]^+$; **g)** glutathione $[M+H]^+$, glycochenodeoxycholate $[M+H]^+$; **h)** raffinose $[M+H]^+$, probucol $[M+H]^+$. Significant improvements in detection of standards were observed from mixtures where plasma enhancement is employed.

It is clear, first of all, that the introduction of the active plasma device to the laser ablation sampling region of this ion source results in the detection of a large number of ions resulting from the plasma alone and therefore creates significant 'background' information in the mass spectra recorded. This is particularly evident in the lower *m/z* region data (Figure 3 a), b) e), f) and SI Figure S8). However, in the case of the analytes detected here there appeared to be no confounding peaks for our ions on interest and additionally, above approximately *m/z* 500 the background ion intensity from the plasma becomes much less intense, reducing to almost nothing.

Of the standards included within this solution only three, choline $[M]^+$ (SI Figure S8), lipid PC 34:1 $[M+Na]^+$ and co-enzyme Q10 $[M+H]^+$ were detected without plasma enhancement at the concentrations used (Figure 4d *m/z* 782.57 and 863.69 respectively). With the plasma enhancement 13 of the compounds were detected with a range of ion intensities from ~20 for tryptophan up to ~17,000 for amiodarone which, in common with earlier data appeared to benefit the most from the plasma enhancement. Whilst the absence of these species within the non-plasma spectra means a meaningful enhancement factor can't be calculated it can be assumed that the intensities seen here represent the minimum value these would take and therefore show the significant promise plasma enhancement provides. The ion intensities for co-enzyme Q10 and choline did not show enhancement with co-enzyme Q10 remaining approximately level and choline showing a reduction from ~8000 to no detection in the plasma enhanced data. Further interesting features are seen for ions related to PC 34:1 whereby the $[M+Na]^+$ ion observed both with and without plasma (Figure 3d) with approximately x 4 enhancement is the only non-protonated species observed. Additionally, the $[M+H]^+$ adduct of PC 34:1 is only detected with plasma enhancement (Figure 3d), in common with the other compounds here and drug only data described in section 3.2, of protonation being the primary enhancement seen in positive ion mode. Other possible ions are observed relating to PC 34:1 at *m/z* 723.49, 746.55 and 790.6 of which only the ion at *m/z* 723.5 is detected without plasma enhancement. These ions can be tentatively assigned from mass as $[M\text{-}N(CH_3)_3 +Na]^+$, $[M\text{-}CH_2]^+$ and $[M+CH_2OH]^+$ respectively. Further to this the ion detected at 577.52 is likely a headgroup fragment loss from PC 34:1 $[M- C_6H_{14}NO_4P]^+$ [30] and in this example is only observed with plasma enhancement, though is observed without plasma in the literature including by MS/MS fragmentation of PC 34:1 [31, 32].

3.4. Analysis of murine brain

Murine brain was analysed across in both positive and negative ion mode both with and without plasma ionisation enhancement. Additionally, the plasma was left running at the end of these acquisitions to provide reference spectra for any potentially confounding background ions derived solely from the plasma. Example data from these analyses, in the form of total ion chromatograms and mean spectra, are shown in Figure 4.

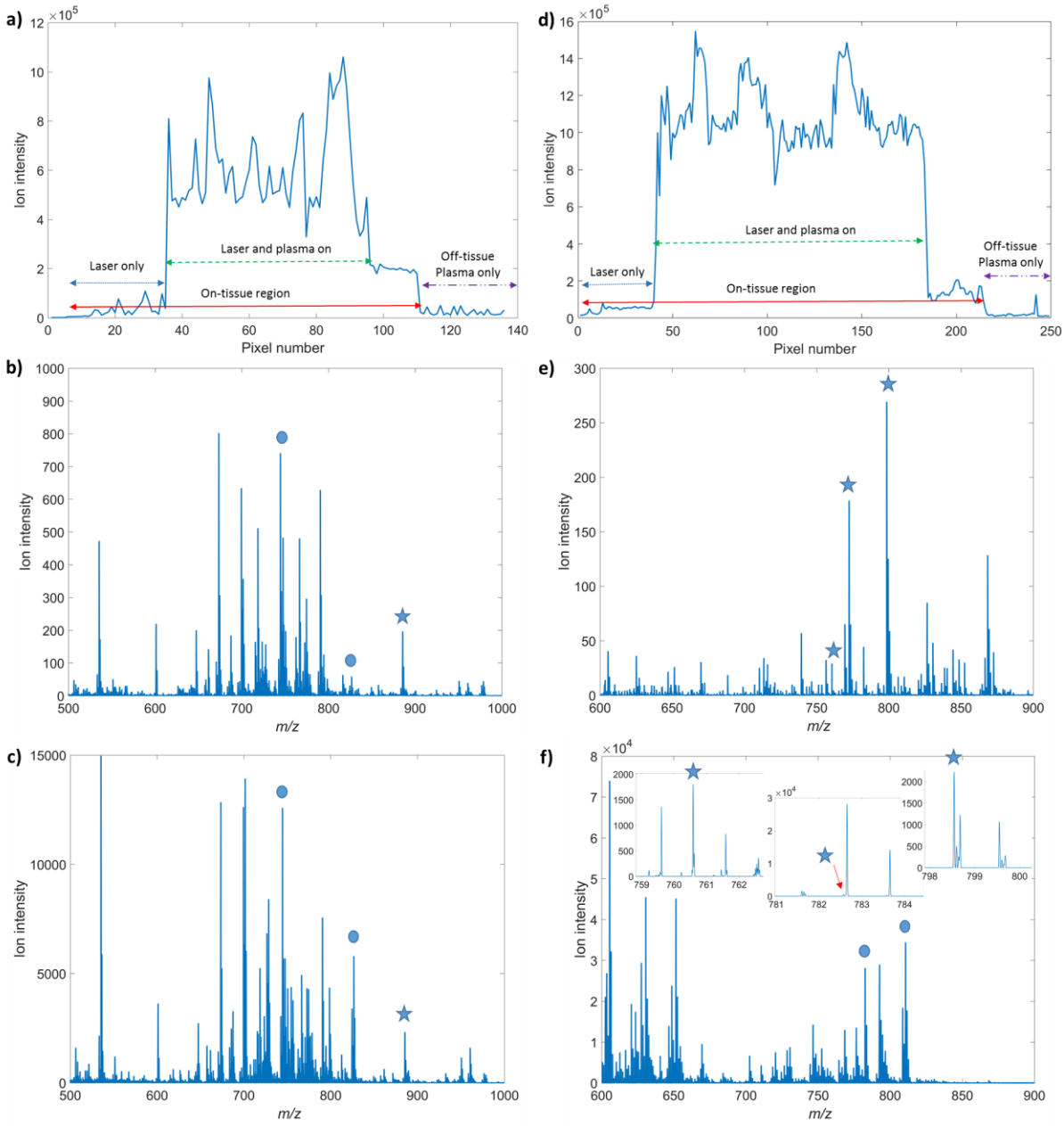

Figure 4. Total ion chromatogram (TIC) from single line raster sample across murine brain tissue in negative (a) and positive (d) ion mode with and without plasma enhancement. Mean spectra overlays from corresponding highlighted TIC regions are shown for negative ion mode (b – laser only, c – laser and plasma) and positive ion (e – laser only, f – laser and plasma). Commonly observed lipid ions in typical MALDI MSI are indicated by stars: *m/z* 885.55 PI 38:4 $[M-H]^-$ in (b, c); *m/z* 760 PC 34:1 $[M+H]^+$, *m/z* 782 $[M+Na]^+$, *m/z* 798 $[M+K]^+$ in (e, f). Other ions of note are labelled by circles and are discussed within the text. Significant enhancement of detected ion intensity is observed with the addition of plasma.

Mean spectra from the indicated regions (Figure 4) were calculated to exemplify the nature of data obtained from analysis of murine brain tissue in continuous raster sampling mode with and without plasma ion enhancement as well as from the plasma only background ions. The TIC plots shown in

Figure 4 a) and d) for negative and positive ion mode respectively indicate the spectra used to calculate each of the subsequent mean spectra overlays in Figure 4 b), c), e) and f). It is clear within the TIC that the switch on of the plasma results in several orders of magnitude increase in total ion count from the tissue signal. Viewed as mean spectra from each region the basepeak for non-plasma enhanced tissue data in the *m/z* 700 – 900 region is approximately 20 and 100 times lower than for the plasma enhanced data in negative and positive ion mode respectively. Of note here is the fact that the plasma enhancement does not simply confer an equal enhancement to all of the peaks present in the non-plasma data but results in the emergence of numerous additional ions, many of which are minimally present within the non-plasma data. To begin to unpick these complex changes the enhancement of ions detected in both plasma and non-plasma enhanced data the example of more commonly detected species can be examined. Within murine brain analysed by MALDI MS commonly observed species are PC 34:1 in positive ion mode and PI 38:4 in negative ion mode [33-36] and these comprise the base peak lipids in their corresponding non-plasma enhanced tissue spectra. Here we observe an increase in ion intensity in the PI 38:4 $[M-H]^-$ by approximately by ~10 times, PC 34:1 $[M+H]^+$ by ~60, $[M+Na]^+$ by ~12 and $[M+K]^+$ by ~8. Looking to the most intense ions within the plasma enhanced data, less commonly reported species are observed with significant enhancement. For example, in positive ion mode two of the most intense ions observed at *m/z* 782.65 and 810.68 and exhibit enhancements of ~1700 and ~2000 respectively compared to non-plasma enhanced data. These ions are assigned by accurate mass as GlcCer(18:1/22:1) $[M+H]^+$ and GlcCer(18:1/24:1) $[M+H]^+$. MS/MS with collision induced dissociation (CID) was carried out for a number of these ions to provide further detail regarding their assignment with other GlcCer structural assignments being evidenced for *m/z* at 810.68, 808.68, 782.66 and 726.59 (SI Figures S9-S15) [37]. Similarly, within the negative ion data ions indicated within Figure 4 b) and c) at *m/z* 744.56 PE(36:1) and 826.67 GlcCer(18:1/24:1) $[M-HO]^-$ are enhanced by ~17 and 100 times respectively. However, the enhancement seen in negative ion mode is possibly more akin to a global intensity increase whereby similar ionic species are comparatively prominent both with and without plasma. Despite the substantial influence of the plasma in these data the influence of the matrix in dictating the identity of the species ionised is not to be overlooked [38].

These data were further analysed by database matching against the human metabolome database (HMDB) [26] to provided tentative assignment by *m/z* to larger numbers of the detected ions (SI Figures S16 and S17). Positive ion mode with plasma results in 418 assigned ions and without plasma gives 100 of which 46 are detected in both modes. For negative ion data where plasma enhancement was applied 665 ions have identities assigned compared to 181 without plasma where 151 are detected in both modes. This further accentuates the apparent differences shown in Figure 4 whereby similar ions are present within both datasets but significant enhancement of ion intensity along with a shift in the dominant species ionised and detected where the plasma enhancement is employed.

Having established these striking improvements, the utility of this ion source for tissue imaging with plasma enhancement was investigated. Example images from positive and negative ion mode at 50 µm square pixel size and positive ion mode at 10 µm square are shown in Figure 5.

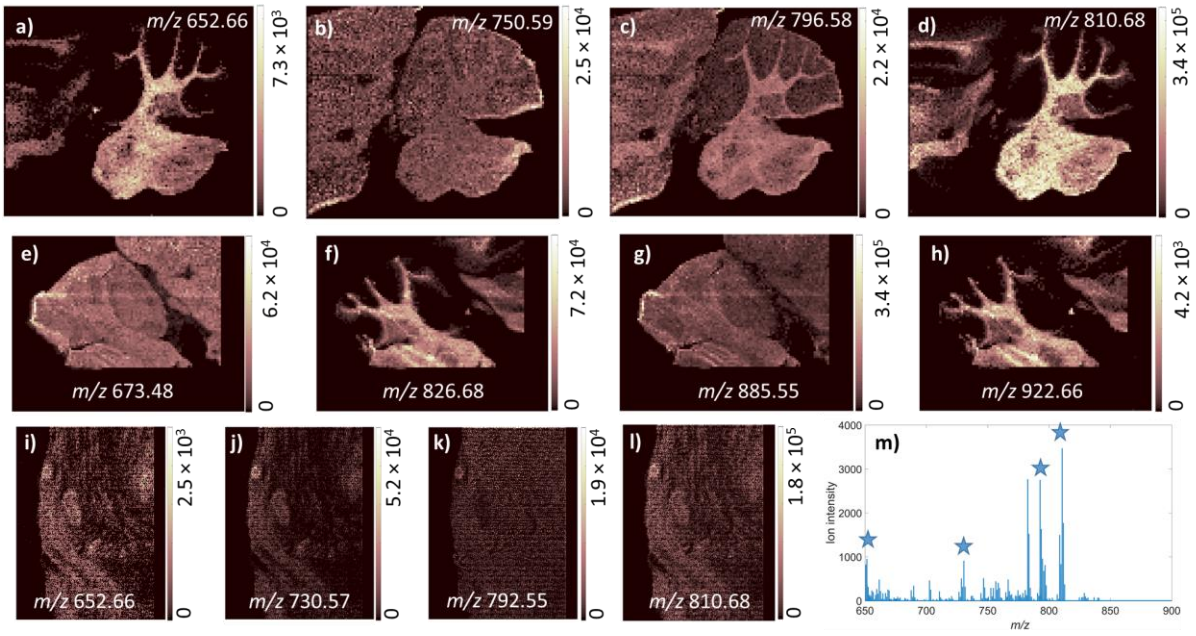

Figure 5. Example single ion images from murine brain tissue section using AP-TM-MALDI-MSI with plasma enhancement. Positive ion (a-d) at 50 µm, negative ion (e-h) at 50 µm and positive ion at 10 µm pixel size (i-l) and a single pixel mass spectrum from the 10 µm data is shown in m). Ions displayed in i) – l) are starred in m) for reference.

Numerous images of apparent high quality were visible within these datasets in both positive and negative ion mode. Data shown in Figure 5 are from ions assigned by *m/z* as **a)** Cer(d18:0/24:0) $[M+H]^+$, **b)** GalCer(d18:1/18:0) $[M+Na]^+$, **c)** PE(40:4) $[M+H]^+$, **d)** GalCer(d18:1/24:1) $[M+H]^+$, **e)** PA (34:1) $[M-H]^-$, **f)** GalCer(d18:1/24:1) $[M-OH]^-$, **g)** PI(38:4) $[M-H]^-$, **h)** PS(46:4) $[M-H]^-$, **i)** Cer(d18:0/24:0) $[M+H]^+$, **j)** PE(P-36:1) $[M+H]^+$, **k)** PE(40:6) $[M+H]^+$, **l)** GalCer(d18:1/24:1) $[M+H]^+$. Interestingly the tissue features and edges within these datasets show no signs of the carryover observed within section 3.2 suggesting the concentrations of these ions or their physicochemical properties are such that any potential issue is minimised.

4. Discussion

It is clear from these data that significant enhancements in detected ion intensity are achieved in both positive and negative ion mode and the AP-TM-MALDI-MSI source constructed here can be applied to imaging thin tissue sections. The enhancements observed appear to be selective to some degree, presumably based on the physico-chemical properties of each analyte molecule / class. This is most striking in positive ion mode where, despite a global enhancement of the ions detected, a substantial change in the most dominant classes of detected ions is observed where plasma enhancement is active. Most significantly, perhaps, is the GalCer class enhancement Notably, some GlcCers were also significantly enhanced by laser post-ionisation in the form of MALDI-2 [39] and whilst the detection of GalCer ions in MSI is not unique to these studies, their detection typically requires non-standard sample preparation such as the use of on-tissue chemistry or silver

nanoparticles [40, 41]. These non-standard preparations often then prevent the detection of the previously abundant species. Here, the extent to which these ions are detected alongside more commonly encountered species here is striking.

There is little published data utilizing plasmas or plasma enhancement in MSI. Bowfield *et al.* demonstrated the use of a micro-plasma device as the primary desorption mechanism for MSI [10]. Recent studies from the Moon group [19, 32] have shown the use of an atmospheric pressure transmission mode laser desorption ionisation source with plasma and nanoparticle enhancement of ionisation labelled as AP-nanoPALDI MS. Within those studies MSI data from tissue were obtained with pixel size down to 1.4 × 5 μm. This system bears similarities to that shown here but despite the ~2 μm lateral resolution shown, does not currently enable effective ionisation of intact species with *m/z* above approximately 600 Daltons. Within the data presented here good quality single pixel spectra were obtained for pixel size of 10 × 10 μm. Therefore, of significant future interest will be the development of sample preparation and laser delivery to best take advantage of the demonstrated benefits of plasma enhancement, further reducing the available pixel sizes accessible to this system within tissue imaging studies. Additionally, further characterisation of any ionisation biases and formation of lesser observed ion adduct forms will need to be carried out.

5. Conclusions

An AP-TM-MALDI-MS ion source was constructed and initial testing and experiments carried out. The open and flexible architecture of the beam delivery and sample scanning system enable a variety of modifications or additions to be made. This, coupled to the high mass resolution and accuracy afforded by an Orbitrap mass spectrometry instrument will enable a wide variety of applied, metrological and fundamental studies to be carried out in AP-TM-MALDI-MSI.

Enhancement of detected ion intensity by plasma post ionisation is shown for the first time in transmission geometry within tissue imaging studies for intact lipid species up to 1000 Daltons. The high quality spectral and imaging data obtained with plasma enhancement demonstrates this post-ionisation method to have real potential for regular use in high resolution tissue imaging studies, with improvements of over three orders of magnitude being evidenced here.

Future work will seek to address the study and optimisation of sample preparation, laser irradiation, inlet heating and plasma device geometry and electoral properties to further develop the utility of this ion source in applied tissue imaging studies.

6. Acknowledgments

The authors thank Keith Oakes at Elforlight for useful discussion. Funding was provided by NPL strategic research program ‘NiCE MSI’ (SR 116301) and Innovate UK (formerly TSB) award 101788.

7. Conflict of Interest Disclosure

These authors declare no conflict of interest.

8. References

[1] M.M. Nudnova, L. Zhu, R. Zenobi, Active capillary plasma source for ambient mass spectrometry, Rapid Commun Mass Sp, 26 (2012) 1447-1452.
[2] G. Robichaud, J.A. Barry, D.C. Muddiman, IR-MALDESI Mass Spectrometry Imaging of Biological Tissue Sections Using Ice as a Matrix, J Am Soc Mass Spectr, 25 (2014) 1-10.
[3] V.V. Laiko, M.A. Baldwin, A.L. Burlingame, Atmospheric pressure matrix-assisted laser desorption/ionization mass spectrometry, Anal Chem, 72 (2000) 652-657.
[4] A. Koch, A. Schnapp, J. Soltwisch, K. Dreisewerd, Generation of multiply charged peptides and proteins from glycerol-based matrices using lasers with ultraviolet, visible and near-infrared wavelengths and an atmospheric pressure ion source, Int J Mass Spectrom, 416 (2017) 61-70.
[5] O.J. Hale, P. Ryumin, J.M. Brown, M. Morris, R. Cramer, Production and analysis of multiply charged negative ions by liquid atmospheric pressure matrix-assisted laser desorption/ionization mass spectrometry, Rapid Commun Mass Sp, (2018).
[6] D.R. Bhandari, M. Schott, A. Römpp, A. Vilcinskas, B. Spengler, Metabolite localization by atmospheric pressure high-resolution scanning microprobe matrix-assisted laser desorption/ionization mass spectrometry imaging in whole-body sections and individual organs of the rove beetle Paederus riparius, Anal Bioanal Chem, (2014) 1-13.
[7] S. Guenther, A. Römpp, W. Kummer, B. Spengler, AP-MALDI imaging of neuropeptides in mouse pituitary gland with 5µm spatial resolution and high mass accuracy, Int J Mass Spectrom, 305 (2011) 228-237.
[8] B. Spengler, M. Hubert, Scanning microprobe matrix-assisted laser desorption ionization (SMALDI) mass spectrometry: instrumentation for sub-micrometer resolved LDI and MALDI surface analysis, J Am Soc Mass Spectr, 13 (2002) 735-748.
[9] X. Ding, Y. Duan, Plasma-based ambient mass spectrometry techniques: the current status and future prospective, Mass spectrometry reviews, 34 (2015) 449-473.
[10] A. Bowfield, J. Bunch, T.L. Salter, R.T. Steven, I.S. Gilmore, D.A. Barrett, M.R. Alexander, K. McKay, J.W. Bradley, Characterisation of a micro-plasma for ambient mass spectrometry imaging, Analyst, 139 (2014) 5430-5438.
[11] J.K. Dalgleish, M. Wleklinski, J.T. Shelley, C.C. Mulligan, Z. Ouyang, R. Graham Cooks, Arrays of low-temperature plasma probes for ambient ionization mass spectrometry, Rapid Commun Mass Sp, 27 (2013) 135-142.
[12] B. Vortmann, S. Nowak, C. Engelhard, Rapid characterization of lithium ion battery electrolytes and thermal aging products by low-temperature plasma ambient ionization high-resolution mass spectrometry, Anal Chem, 85 (2013) 3433-3438.
[13] T.L.R. Salter, J. Bunch, I.S. Gilmore, Importance of sample form and surface temperature for analysis by ambient plasma mass spectrometry (PADI), Anal Chem, 86 (2014) 9264-9270.
[14] T.L. Salter, I.S. Gilmore, A. Bowfield, O.T. Olabanji, J.W. Bradley, Ambient Surface Mass Spectrometry Using Plasma-Assisted Desorption Ionization: Effects and Optimization of Analytical Parameters for Signal Intensities of Molecules and Polymers, Anal Chem, 85 (2013) 1675-1682.
[15] A. Zavalin, J. Yang, K. Hayden, M. Vestal, R.M. Caprioli, Tissue protein imaging at 1 µm laser spot diameter for high spatial resolution and high imaging speed using transmission geometry MALDI TOF MS, Anal Bioanal Chem, 407 (2015) 2337-2342.
[16] A. Zavalin, E.M. Todd, P.D. Rawhouser, J. Yang, J.L. Norris, R.M. Caprioli, Direct imaging of single cells and tissue at sub-cellular spatial resolution using transmission geometry MALDI MS, J Mass Spectrom, 47 (2012) 1473-1481.

[17] S. Trimpin, T.N. Herath, E.D. Inutan, S.A. Cernat, J.B. Miller, K. Mackie, J.M. Walker, Field-free transmission geometry atmospheric pressure matrix-assisted laser desorption/ionization for rapid analysis of unadulterated tissue samples, Rapid Commun Mass Sp, 23 (2009) 3023-3027.
[18] A.L. Richards, C.B. Lietz, J.B. Wager-Miller, K. Mackie, S. Trimpin, Imaging mass spectrometry in transmission geometry, Rapid Commun Mass Sp, 25 (2011) 815-820.
[19] J.Y. Kim, E.S. Seo, H. Kim, J.-W. Park, D.-K. Lim, D.W. Moon, Atmospheric pressure mass spectrometric imaging of live hippocampal tissue slices with subcellular spatial resolution, Nature communications, 8 (2017) 2113.
[20] M.C. Galicia, A. Vertes, J.H. Callahan, Atmospheric pressure matrix-assisted laser desorption/ionization in transmission geometry, Anal Chem, 74 (2002) 1891-1895.
[21] B.B. Schneider, C. Lock, T.R. Covey, AP and vacuum MALDI on a QqLIT instrument, J Am Soc Mass Spectr, 16 (2005) 176-182.
[22] R.T. Steven, A. Dexter, J. Bunch, Investigating MALDI MSI parameters (Part 1)–A systematic survey of the effects of repetition rates up to 20kHz in continuous raster mode, Methods, (2016).
[23] R.T. Steven, A.M. Race, J. Bunch, Probing the Relationship Between Detected Ion Intensity, Laser Fluence, and Beam Profile in Thin Film and Tissue in MALDI MSI, J Am Soc Mass Spectr, 27 (2016) 1419-1428.
[24] M.C. Chambers, B. Maclean, R. Burke, D. Amodei, D.L. Ruderman, S. Neumann, L. Gatto, B. Fischer, B. Pratt, J. Egertson, A cross-platform toolkit for mass spectrometry and proteomics, Nature biotechnology, 30 (2012) 918-920.
[25] A.M. Race, A.D. Palmer, A. Dexter, R.T. Steven, I.B. Styles, J. Bunch, SpectralAnalysis: Software for the Masses, Anal Chem, 88 (2016) 9451-9458.
[26] D.S. Wishart, Y.D. Feunang, A. Marcu, A.C. Guo, K. Liang, R. Vázquez-Fresno, T. Sajed, D. Johnson, C. Li, N. Karu, HMDB 4.0: the human metabolome database for 2018, Nucleic acids research, 46 (2017) D608-D617.
[27] R.T. Steven, A. Dexter, J. Bunch, Investigating MALDI MSI parameters (Part 2)–On the use of a mechanically shuttered trigger system for improved laser energy stability, Methods, (2016).
[28] B. Prideaux, M. Stoeckli, Mass spectrometry imaging for drug distribution studies, Journal of proteomics, 75 (2012) 4999-5013.
[29] K. McKay, T.L. Salter, A. Bowfield, J.L. Walsh, I.S. Gilmore, J.W. Bradley, Comparison of three plasma sources for ambient desorption/ionization mass spectrometry, J Am Soc Mass Spectr, 25 (2014) 1528-1537.
[30] K.A. Zemski Berry, J.A. Hankin, R.M. Barkley, J.M. Spraggins, R.M. Caprioli, R.C. Murphy, MALDI Imaging of Lipid Biochemistry in Tissues by Mass Spectrometry, Chem Rev, 111 (2011) 6491-6512.
[31] R.T. Steven, A.M. Race, J. Bunch, Para-Nitroaniline is a promising matrix for MALDI-MS imaging on intermediate pressure MS systems, J Am Soc Mass Spectr, 24 (2013) 801-804.
[32] J.Y. Kim, S.Y. Lee, H. Kim, J.-W. Park, D.-K. Lim, D.W. Moon, Biomolecular Imaging of Regeneration of Zebrafish Caudal Fins using High Spatial Resolution Ambient Mass Spectrometry, Anal Chem, (2018).
[33] R.T. Steven, J. Bunch, Repeat MALDI MS imaging of a single tissue section using multiple matrices and tissue washes, Anal Bioanal Chem, 405 (2013) 4719-4728.
[34] A.M. Hicks, C.J. DeLong, M.J. Thomas, M. Samuel, Z. Cui, Unique molecular signatures of glycerophospholipid species in different rat tissues analyzed by tandem mass spectrometry, Biochimica et Biophysica Acta (BBA)-Molecular and Cell Biology of Lipids, 1761 (2006) 1022-1029.
[35] S. Shimma, A. Kubo, T. Satoh, M. Toyoda, Detailed structural analysis of lipids directly on tissue specimens using a MALDI-SpiralTOF-Reflectron TOF mass spectrometer, PLoS One, 7 (2012) e37107.
[36] N. Zaima, S. Yoshioka, Y. Sato, S. Shinano, Y. Ikeda, T. Moriyama, Enhanced specificity for phosphatidylcholine analysis by positive ion mode matrix-assisted laser desorption/ionization imaging mass spectrometry, Rapid Commun Mass Sp, 28 (2014) 1453-1458.
[37] F. Allen, R. Greiner, D. Wishart, Competitive fragmentation modeling of ESI-MS/MS spectra for putative metabolite identification, Metabolomics, 11 (2015) 98-110.

[38] S.N. Jackson, L. Muller, A. Roux, B. Oktem, E. Moskovets, V.M. Doroshenko, A.S. Woods, AP-MALDI Mass Spectrometry Imaging of Gangliosides Using 2, 6-Dihydroxyacetophenone, J Am Soc Mass Spectr, 29 (2018) 1463-1472.
[39] J. Soltwisch, H. Kettling, S. Vens-Cappell, M. Wiegelmann, J. Müthing, K. Dreisewerd, Mass spectrometry imaging with laser-induced postionization, Science, (2015) aaa1051.
[40] L. Muller, K. Baldwin, D.C. Barbacci, S.N. Jackson, A. Roux, C.D. Balaban, B.E. Brinson, M.I. McCully, E.K. Lewis, J.A. Schultz, Laser desorption/ionization mass spectrometric imaging of endogenous lipids from rat brain tissue implanted with silver nanoparticles, J Am Soc Mass Spectr, 28 (2017) 1716-1728.
[41] S. Vens-Cappell, I.U. Kouzel, H. Kettling, J. Soltwisch, A. Bauwens, S. Porubsky, J. Müthing, K. Dreisewerd, On-tissue phospholipase C digestion for enhanced MALDI-MS imaging of neutral glycosphingolipids, Anal Chem, 88 (2016) 5595-5599.